Two tyrosine residues, Tyr-108 and Tyr-503, are responsible for the deprotonation of phenolic substrates in vanillyl-alcohol oxidase

Ewing, Tom A; Nguyen, Quoc-Thai; Allan, Robert C; Gygli, Gudrun; Romero, Elvira; Binda, Claudia; Fraaije, Marco W; Mattevi, Andrea; van Berkel, Willem J H

Published in:
The Journal of Biological Chemistry

DOI:
10.1074/jbc.M117.778449

Publication date:
2017

Two tyrosine residues, Tyr-108 and Tyr-503, are responsible for the deprotonation of phenolic substrates in vanillyl-alcohol oxidase

Received for publication, February 10, 2017, and in revised form, July 5, 2017 Published, Papers in Press, July 17, 2017, DOI 10.1074/jbc.M117.778449

Tom A. Ewing[‡], Quoc-Thai Nguyen[§¶‖], Robert C. Allan[‡], Gudrun Gygli[‡], Elvira Romero[¶], Claudia Binda[§], Marco W. Fraaije[¶], Andrea Mattevi[§], and Willem J. H. van Berkel[‡1]

From the [‡]Laboratory of Biochemistry, Wageningen University & Research, Stippeneng 4, 6708 WE Wageningen, The Netherlands, the [§]Department of Biology and Biotechnology, University of Pavia, Via Ferrata 9, 27100 Pavia, Italy, the [¶]Molecular Enzymology Group, University of Groningen, Nijenborgh 4, 9747 AG Groningen, The Netherlands, and the [‖]Faculty of Pharmacy, University of Medicine and Pharmacy, 41 Dinh Tien Hoang Street, Ben Nghe Ward, District 1, Ho Chi Minh City, Vietnam

Edited by F. Peter Guengerich

A number of oxidoreductases from the VAO/*para*-cresol methylhydroxylase flavoprotein family catalyze the oxidation of *para*-substituted phenols. One of the best-studied is vanillyl-alcohol oxidase (VAO) from the fungus *Penicillium simplicissimum*. For oxidation of phenols by VAO to occur, they must first be bound in the active site of the enzyme in their phenolate anion form. The crystal structure of VAO reveals that two tyrosine residues, Tyr-108 and Tyr-503, are positioned to facilitate this deprotonation. To investigate their role in catalysis, we created three VAO variants, Y108F, Y503F, and Y108F/Y503F, and studied their biochemical properties. Steady-state kinetics indicated that the presence of at least one of the tyrosine residues is essential for efficient catalysis by VAO. Stopped-flow kinetics revealed that the reduction of VAO by chavicol or vanillyl alcohol occurs at two different rates: k_{obs1}, which corresponds to its reaction with the deprotonated form of the substrate, and k_{obs2}, which corresponds to its reaction with the protonated form of the substrate. In Y108F, Y503F, and Y108F/Y503F, the relative contribution of k_{obs2} to the reduction is larger than in wild-type VAO, suggesting deprotonation is impaired in these variants. Binding studies disclosed that the competitive inhibitor isoeugenol is predominantly in its deprotonated form when bound to wild-type VAO, but predominantly in its protonated form when bound to the variants. These results indicate that Tyr-108 and Tyr-503 are responsible for the activation of substrates in VAO, providing new insights into the catalytic mechanism of VAO and related enzymes that oxidize *para*-substituted phenols.

Vanillyl-alcohol oxidase (VAO)[2] (EC 1.1.3.38) from *Penicillium simplicissimum* is a flavin-dependent oxidase that catalyzes the oxidation of *para*-substituted phenolic compounds using molecular oxygen as an electron acceptor (1–3). It is a 64-kDa (560 amino acid) protein that forms octameric structures with each subunit containing an FAD cofactor that is covalently linked to the protein via an 8α-*N*3-histidyl-FAD bond (4). VAO is a member of the VAO/*para*-cresol methylhydroxylase (PCMH) flavoprotein family, which consists of homologous oxidoreductases that catalyze a wide range of reactions, but share a conserved FAD-binding domain (5). Although VAO catalyzes a range of reactions, such as the oxidation of benzylic alcohols to aldehydes, the oxidative deamination of benzylic amines, the hydroxylation of 4-allylphenols, and the hydroxylation or dehydrogenation of 4-alkylphenols, it displays a strict selectivity toward the oxidation of *para*-substituted phenols at the Cα atom of their side chain. The proposed catalytic mechanism of VAO provides an explanation for this selectivity (Fig. 1*A*) (2, 6, 7). First, the substrates of VAO are bound in the active site in their deprotonated phenolate form. Subsequently, a hydride anion is transferred from the Cα atom of the side chain of the substrate to the N5 atom of FAD, yielding the reduced enzyme and a *para*-quinone methide intermediate. Finally, this intermediate either reacts with water or rearranges to yield the product of the reaction, and FAD is reoxidized by molecular oxygen, which is converted to hydrogen peroxide. The initial deprotonation of the phenolic hydroxyl group of the substrate is likely a crucial step in this mechanism, as it promotes the hydride-transfer reaction by enabling the formation of the *para*-quinone methide intermediate. Studies using the competitive inhibitor isoeugenol (Fig. 1*B*) revealed that its pK_a is lowered from 10 to 5 upon binding to VAO (2). A potential explanation for this decrease is provided by examining the crystal structure of VAO in complex with isoeugenol (4). Three polar residues, Tyr-108, Tyr-503, and Arg-504, form a phenolate-binding pocket, with their side chains positioned within hydrogen bonding distance of phenolic hydroxyl group of the isoeugenol (Fig. 2*A*). These residues may facilitate deprotonation of the substrate either by promoting preferential binding of the deprotonated form or by one of the tyrosine residues acting as a base and actively deprotonating the substrate in the active site. All three residues are conserved in the homologous flavoenzymes eugenol oxidase (EUGO) and

This work was supported by European Union through the INDOX project FP7-KBBE-2013-7-613549. The authors declare that they have no conflicts of interest with the contents of this article.

The atomic coordinates and structure factors (codes 5MXJ and 5MXU) have been deposited in the Protein Data Bank (http://wwpdb.org/).

[1] To whom correspondence should be addressed: Stippeneng 4, 6708 WE, Wageningen, The Netherlands. Tel.: 31-317-482861; Fax: 31-317-484801; E-mail: willem.vanberkel@wur.nl.

[2] The abbreviations used are: VAO, vanillyl-alcohol oxidase; 4PO, 4-phenol oxidizing; EUGO, eugenol oxidase; PCMH, *para*-cresol methylhydroxylase; r.m.s., root mean square; PDB, Protein Data Bank.

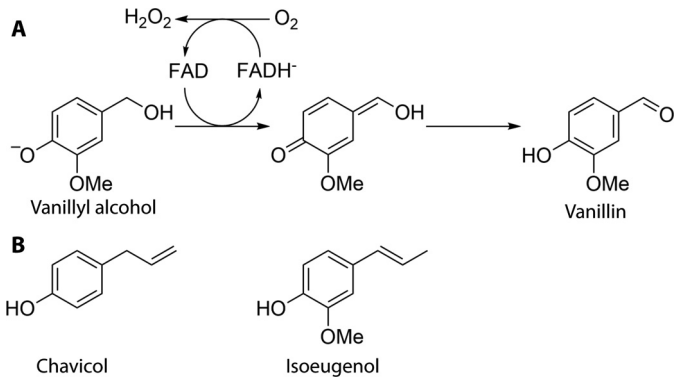

Figure 1. *A,* oxidation of vanillyl alcohol as catalyzed by VAO. First, the substrate is bound in the active site in its deprotonated phenolate form. This facilitates the transfer of a hydride anion from the Cα of the substrate to FAD, yielding a *para*-quinone methide intermediate and the reduced enzyme. This intermediate subsequently rearranges to give the aldehyde product vanillin and FAD is reoxidized by molecular oxygen, which is converted to hydrogen peroxide. *B,* structures of chavicol and isoeugenol.

para-cresol methylhydroxylase (PCMH, EC 1.17.99.1), which also catalyze the oxidation of *para*-substituted phenols (8, 9). The role of Arg-474 in PCMH, which corresponds to Arg-504 in VAO, has been studied by site-directed mutagenesis and it was found to be of importance in achieving covalent incorporation of the cofactor of the enzyme and in enabling efficient catalysis by modulating the redox properties of both the cofactor and enzyme-bound substrates (10). Here, we investigated the role played by Tyr-108 and Tyr-503 in VAO using site-directed mutagenesis. Three VAO variants, Y108F, Y503F, and Y108F/Y503F, were created, expressed, and purified and their catalytic properties were studied. Our results reveal that the presence of at least one of these tyrosine residues is essential for efficient catalysis.

Results

The Y108F, Y503F, and Y108F/Y503F variants were successfully expressed in *Escherichia coli* and purified. Like wild-type (wt)-VAO, all three variants contained a covalently bound FAD cofactor, as judged from the yellow pellet and colorless supernatant obtained after precipitation of the proteins with trichloroacetic acid. In their native form, all variants displayed an octameric quaternary structure, as demonstrated by analytical size exclusion chromatography (data not shown). The flavin absorption spectra of the variants were highly similar to that of wt-VAO (see spectral studies presented below), demonstrating that the introduced mutations do not lead to any major changes in the electronic environment of their flavin cofactor. To determine whether the introduced mutations affect the stability of VAO, thermal midpoints of unfolding of the variants were determined using the ThermoFAD method (11). This yielded thermal midpoints of unfolding of 55 °C for wt-VAO, 53 °C for Y108F and Y503F, and 52 °C for Y108F/Y503F, suggesting the introduced mutations have a minor deleterious effect on the thermostability of VAO.

Steady-state catalytic properties

To determine the effect of the introduced mutations on the catalytic efficiency of VAO, we measured the apparent steady-

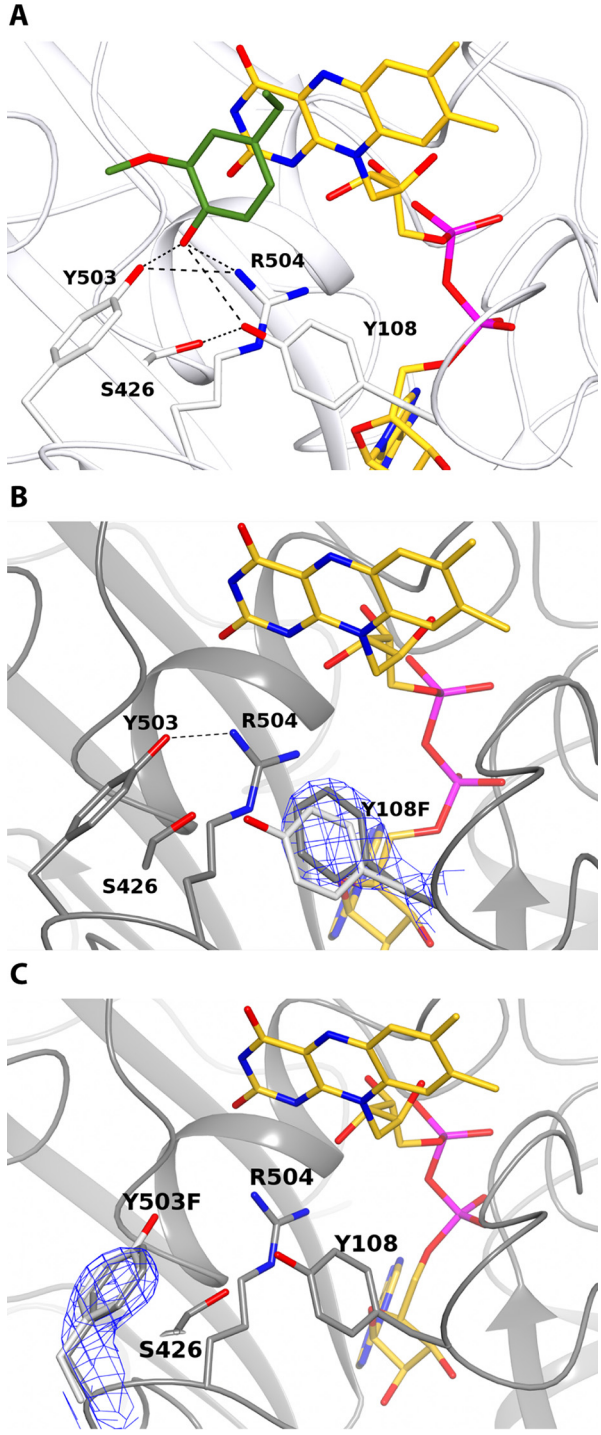

Figure 2. Structure of the phenolate-binding pocket of VAO in the wild-type enzyme (*A*, carbon in *white* (PDB code 2VAO (4))) and in the Y108F and Y503F variants (*B* and *C*, respectively, carbon in *gray*). The refined $2F_o - F_c$ electron density map (contoured at 1.2σ) is shown for the mutated residues Y108F and Y503F as *blue chicken-wire*. The wt-VAO crystal structure in complex with the competitive inhibitor isoeugenol (*A*, carbon in *green*) is taken as a reference to analyze the mutant proteins. As reported in Ref. 4, binding of isoeugenol does not significantly influence the geometry of the active site. In *B* and *C*, the side chains of Tyr-108 and Tyr-503, respectively, from wt-VAO are shown for comparison. As described in the text, in the Y503F mutant Phe-503 is slightly tilted with respect to the corresponding Tyr-503 in wt-VAO. Tyr-108, Tyr-503, Arg-504, Ser-426, isoeugenol, and the FAD cofactor (carbon in *yellow*) are displayed in stick representation with the surrounding protein backbone shown in schematic representation. Oxygen atoms are in *red*, nitrogen atoms in *blue*, and phosphorous atoms in *magenta*. Potential hydrogen bonds are depicted as *black dashed lines*.

Table 1

Apparent steady-state kinetic parameters for the oxidation of vanillyl alcohol and chavicol by VAO variants

Kinetic parameters were determined at 25 °C in 50 mM potassium phosphate buffer, pH 7.5. K_i is the inhibition constant for substrate inhibition, which was observed for all variants when using chavicol as a substrate.

VAO variant	k_{cat}	K_m	k_{cat}/K_m	K_i
	s^{-1}	μM	s^{-1} mM^{-1}	mM
Vanillyl alcohol				
Wild Type	2.6[a]	149[a]	17	
Y108F	0.042 ± 0.006	1750 ± 420	0.024	
Y503F	0.055 ± 0.002	990 ± 60	0.056	
Y108F/Y503F	ND[b]	ND	ND	
Chavicol				
Wild Type	7.4 ± 0.1	6.5 ± 0.3	1138	7.0 ± 1.1
Y108F	3.4 ± 0.1	67 ± 7	51	2.9 ± 0.4
Y503F	3.3 ± 0.1	21 ± 2	157	0.45 ± 0.04
Y108F/Y503F	0.13 ± 0.01	74 ± 6	1.8	1.4 ± 0.2

[a] Data were taken from Ref. 14.
[b] ND, not determined due to low reaction rate (observed rate <0.01 s^{-1} at 2 mM vanillyl alcohol concentration).

Table 2

Observed rates of reduction of VAO variants by 2 mM vanillyl alcohol

Rates were determined by fitting appropriate exponential functions to single wavelength traces of the absorption at 439 nm obtained after mixing 10 μM enzyme with 2 mM vanillyl alcohol in 50 mM potassium phosphate buffer, pH 6.2 or 7.5, under anaerobic conditions at 25 °C using a stopped-flow apparatus. Values in parentheses give the relative contribution of k_{obs1} and k_{obs2}, the two phases associated with flavin reduction, to the drop in absorption. The observed rates for the oxidation of 2 mM vanillyl alcohol under steady-state conditions (k_{ss}) at pH 7.5 are given for comparison.

VAO variant	k_{obs1}	k_{obs2}	k_{ss}
	s^{-1}		
pH 7.5			
Wild Type	27 ± 1 (0.67)	3.5 ± 0.1 (0.33)	2.4
Y108F	0.061 ± 0.002 (0.17)	0.023 ± 0.001 (0.83)	0.024
Y503F	0.075 ± 0.001 (0.26)	0.025 ± 0.001 (0.74)	0.037
Y108F/Y503F	ND[a]	ND	<0.01
pH 6.2			
Wild Type	35 ± 1 (0.23)	2.9 ± 0.1 (0.77)	
Y108F	0.27 ± 0.01 (0.03)	0.0085 ± 0.0001 (0.97)	
Y503F	0.33 ± 0.01 (0.03)	0.018 ± 0.001 (0.97)	
Y108F/Y503F	ND	ND	

[a] ND, not determined due to low reaction rate.

state kinetic parameters for the oxidation of two substrates: vanillyl alcohol, which is oxidized to the aldehyde vanillin, and chavicol (Fig. 1*B*), which is hydroxylated to coumaryl alcohol. The kinetic parameters for the oxidation of these substrates are listed in Table 1. Interestingly, the effect of the mutations varied depending on the substrate. With vanillyl alcohol, the k_{cat} drops to ~2% of that of wt-VAO for both the Y108F and Y503F variants. With chavicol, a more minor drop in the k_{cat} value to ~45% of that of the wild-type enzyme was observed for the Y108F and Y503F variants. With chavicol, the Y108F/Y503F variant displayed a k_{cat} value of less than 2% of that of wt-VAO and with vanillyl alcohol, the activity was too low to accurately determine kinetic parameters. This indicates that the presence of at least one of the two tyrosine residues is essential for effective catalysis. For each variant, the K_m increased for each substrate. The magnitude of the increase ranged from 3- to 12-fold.

Stopped-flow kinetics of the reductive half-reaction

To determine whether the decreased catalytic efficiencies observed for the VAO variants were due to impaired reduction of their FAD cofactor, spectral changes during the anaerobic reduction of the enzymes by vanillyl alcohol or chavicol were followed by stopped-flow spectroscopy. Where possible, photodiode array detection was used to monitor changes over a spectral range from 254 to 725 nm. However, with long measurement times (>10 s), the high-intensity illumination required for this led to photoreduction of FAD. Therefore, in cases where the reduction reaction was slow, it was monitored using single wavelength detection at 439 nm, the absorption maximum of the oxidized FAD in VAO. This was the case for the reduction of the Y108F and Y503F variants by 2 mM vanillyl alcohol and for all reactions involving the Y108F/Y503F variant.

Observed rates for the anaerobic reduction of wt-VAO and the Y108F and Y503F variants by 2 mM vanillyl alcohol at pH 6.2 and 7.5 are given in Table 2. The anaerobic reduction of wt-VAO by vanillyl alcohol at pH 7.5 has been studied previously and was found to be a biphasic process with rate constants at saturating substrate concentrations of k_{red1} = 24 s^{-1} and k_{red2} = 3.5 s^{-1} (6). The two different rates of reduction were interpreted to be caused by the presence of two conformations of the enzyme. The rate of the slower phase, k_{red2}, lies close to k_{cat} and is rate-limiting for catalysis. Our results with wt-VAO are in good agreement with these data. The effect of the Y108F and Y503F mutations on the rate of reduction by vanillyl alcohol was similar. In each variant, the reduction was a biphasic process. Each of the rates of reduction has dropped significantly as compared with wt-VAO. The rates of the two phases are in the same range and k_{obs2} is similar to the rate of steady-state catalysis, suggesting that flavin reduction is rate-limiting in these variants. In addition to the decrease in both reduction rates, the relative contribution of the two kinetic events to the drop in absorption at 439 nm (amplitude *a*) has changed. In wt-VAO, k_{obs1} has a greater contribution than k_{obs2} (a_1:a_2 ≈ 2:1), whereas in the Y108F and Y503F variants, k_{obs2} has a greater contribution than k_{obs1} (a_1:a_2 ≈ 1:5 for Y108F and 1:3 for Y503F). At pH 6.2, reduction by vanillyl alcohol was also biphasic for all variants. For wt-VAO, the rates of the two phases are very similar to those at pH 7.5. However, their contributions to the reduction have changed, with k_{obs2} having a greater contribution than k_{obs1} (a_1:a_2 ≈ 1:3). In the Y108F and Y503F variants, k_{obs1} is somewhat higher than observed at pH 7.5 and k_{obs2} is slightly lower in Y108F and does not change significantly in Y503F. As observed for wt-VAO, the contribution of the two rates to the change in absorption shifts, with k_{obs2} becoming more predominant (a_1:a_2 ≈ 1:32 for each variant).

Spectra obtained during the anaerobic reduction of wt-VAO by 100 μM chavicol are shown in Fig. 3. After mixing wt-VAO with chavicol, the characteristic peak of the oxidized flavin cofactor of the enzyme (maximum at 439 nm) rapidly disappears, indicating that FAD is reduced by the substrate. At the same time, the absorption between 320 and 430 nm increases, yielding an intense peak with a maximum at 373 nm. This peak reaches its maximum intensity after ~600 ms, after which it decreases in intensity. The formation of a species with similar spectral characteristics has been observed during the anaerobic reduction of wt-VAO by vanillyl alcohol (λ_{max} = 362 nm) or 4-(methoxymethyl)phenol (λ_{max} = 364 nm) and was attributed to a complex between the quinone methide intermediate and the reduced enzyme formed after the electron-transfer reaction

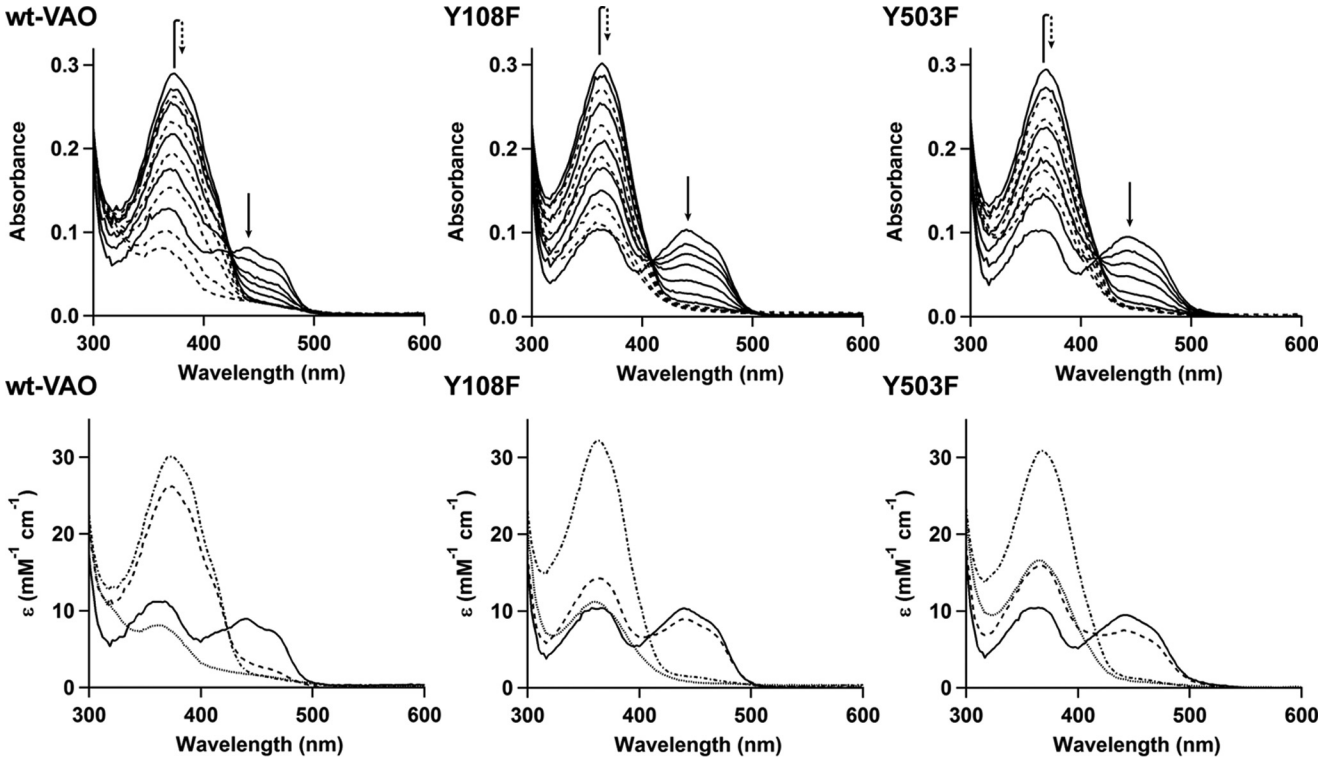

Figure 3. Spectral changes observed during the anaerobic reduction of VAO variants by chavicol. *Top panels* show spectra obtained after mixing 10 μM wt-VAO, Y108F, or Y503F with 100 μM chavicol in a stopped-flow apparatus under anaerobic conditions in 50 mM potassium phosphate buffer, pH 7.5, at 25 °C. Initially, FAD is reduced and a complex between the reduced enzyme and a *para*-quinone methide intermediate is formed (*solid lines*). Subsequently, the *para*-quinone methide intermediate decays, likely due to it reacting with water to yield the product (coumaryl alcohol) and the reduced enzyme (*dashed lines*). For wt-VAO, spectra were obtained 0.001, 0.004, 0.009, 0.019, 0.079, 0.60, 2.3, 4.3, 7.2, 12, 25, and 75 s after mixing. For Y108F, spectra were obtained 0.001, 0.071, 0.17, 0.31, 0.64, 1.1, 2.2, 6.1, 12, 20, 45, and 120 s after mixing. For Y503F, spectra were obtained 0.001, 0.071, 0.17, 0.31, 0.64, 1.1, 5.0, 8.7, 17, 44, and 120 s after mixing. *Bottom panels* show spectra of reaction intermediates obtained after spectral deconvolution of the stopped-flow data for wt-VAO, Y108F, and Y503F. Data were fit to a three-phase model (1→2→3→4), yielding four spectrally distinct species: 1 (—), 2 (- - -), 3 (-·-·-), and 4 (···). One- or two-phase models were not able to satisfactorily explain the data. The rates obtained for the three phases (average of at least 3 measurements) are: $k_1 = 134\ s^{-1}$, $k_2 = 3.7\ s^{-1}$, and $k_3 = 0.093\ s^{-1}$ for wt-VAO, $k_1 = 29\ s^{-1}$, $k_2 = 1.7\ s^{-1}$, and $k_3 = 0.051\ s^{-1}$ for Y108F, and $k_1 = 13\ s^{-1}$, $k_2 = 2.7\ s^{-1}$, and $k_3 = 0.083\ s^{-1}$ for Y503F. These rates are in good agreement with those obtained by fitting to single wavelength traces at 440 nm (see Table 3).

has taken place (6). Intermediate spectra obtained upon spectral deconvolution of the stopped-flow data are shown in Fig. 3. The data were fit to a three-phase consecutive model, yielding four distinct spectral intermediates. Species 1 represents the oxidized enzyme. Species 3 displays the highest absorption at 373 nm and complete loss of the characteristic oxidized flavin spectrum. It likely represents the quinone methide-reduced enzyme complex. Species 2 displays incomplete formation of the quinone methide intermediate as indicated by its lower absorption at 373 nm. In addition, part of the FAD cofactor is still in its oxidized form in this species, as evidenced by the absorption in the range 440–500 nm. The spectra of species 1, 2, and 3 display an isosbestic point at 423 nm and a spectrum calculated by assuming that the spectrum of species 2 is a simple composite of those of species 1 (20%) and 3 (80%) was virtually indistinguishable from the actual spectrum of species 2. This is consistent with species 2 not representing a real reaction intermediate, but rather reflecting the fact that there are two separate rates of conversion of species 1 to species 3. Species 4 displays a spectrum that is typical of a reduced flavoprotein, suggesting that this species is formed by the breakdown of the quinone methide intermediate by its reaction with water, yielding the product coumaryl alcohol. Thus, the anaerobic reduction of wt-VAO by chavicol proceeds as follows. First, the substrate binds to the enzyme. Subsequently, the FAD cofactor is reduced by the substrate leading to the formation of a quinone methide-reduced enzyme complex with two kinetic phases that both contribute to this reduction being distinguished. Following reduction, the quinone methide intermediate reacts with water to yield coumaryl alcohol. Rate constants for these processes were obtained by fitting curves of the absorption at 440 nm to a triphasic exponential function. Rate constants for the two reduction rates (k_{obs1} and k_{obs2}) are given in Table 3. k_{obs2} is similar to the steady-state reaction rate, suggesting it is rate-limiting for catalysis. The observed rate of decay of the quinone methide intermediate, k_{obs3}, was similar for all variants (0.1–0.2 s^{-1}) and is too slow to be catalytically relevant. Presumably, breakdown of this intermediate is faster in the presence of oxygen, as has been observed previously for the quinone methide intermediate formed upon reduction of wt-VAO by 4-(methoxymethyl)phenol (6).

Upon reduction of the Y108F and Y503F variants by chavicol, the spectral changes observed were similar to those seen with wt-VAO, with reduction of FAD occurring concomitantly with the appearance of a putative quinone methide intermediate (Fig. 3). The absorption maximum of this intermediate is shifted to lower wavelengths in the variants (363 nm for Y108F and 368 nm for Y503F) compared with wt-VAO (373 nm).

Table 3

Observed rates of reduction of VAO variants by 100 μM chavicol

Rates were determined by fitting appropriate exponential functions to traces of the absorption at 440 nm (from photodiode array detection (wt-VAO, Y108F, and Y503F)) or 439 nm (from single wavelength detection (Y108F/Y503F)) obtained after mixing 10 μM enzyme with 100 μM chavicol in 50 mM potassium phosphate buffer, pH 6.2 or 7.5, under anaerobic conditions at 25 °C using a stopped-flow apparatus. Values in parentheses give the relative contribution of k_{obs1} and k_{obs2}, the two phases associated with flavin reduction, to the drop in absorption. The observed rates for the oxidation of 100 μM chavicol under steady-state conditions (k_{ss}) at pH 7.5 are given for comparison.

VAO variant	k_{obs1}	k_{obs2}	k_{ss}
		s^{-1}	
pH 7.5			
Wild Type	139 ± 1 (0.76)	4.5 ± 0.1 (0.24)	6.8
Y108F	33 ± 1 (0.13)	1.6 ± 0.1 (0.87)	2.0
Y503F	14 ± 1 (0.07)	2.6 ± 0.1 (0.93)	2.3
Y108F/Y503F	19 ± 1 (0.05)	0.11 ± 0.01 (0.95)	0.069
pH 6.2			
Wild Type	132 ± 1 (0.30)	3.7 ± 0.1 (0.70)	
Y108F	NO[a]	0.79 ± 0.01 (1.00)	
Y503F	NO	1.7 ± 0.1 (1.00)	
Y108F/Y503F	21 ± 1 (0.06)	0.027 ± 0.001 (0.94)	

[a] NO, not observed.

Maximum abundance of the intermediate was observed after 2.2 s for the Y108F variant and after 1.5 s for the Y503F variant, after which the intermediate decays. Spectral deconvolution again revealed a three-phase process (Fig. 3). As with wt-VAO, species 1 and 3 represent the oxidized enzyme and the quinone methide-reduced enzyme complex, respectively. Species 2 again displays an absorption spectrum that is a composite of that of species 1 and 3 and is likely not a real reaction intermediate. Species 4 appears to represent a mixture of quinone methide-reduced enzyme complex and free reduced enzyme. This is likely due to the decay of the quinone methide not being complete at the end of the measurement (120 s). Fitting the data at 440 nm to triple exponential functions revealed that k_{obs1} and k_{obs2} are both decreased in each variant (Table 3). However, neither rate in either variant decreased more than 10-fold. Thus, the effect of the Y108F and Y503F mutations on the rate of reduction of VAO by chavicol is less severe than that on the reduction by vanillyl alcohol (k_{obs1} and k_{obs2} decreased >100-fold in each variant). Interestingly, a similar effect on the relative contributions of k_{obs1} and k_{obs2} to reduction was observed with chavicol as with vanillyl alcohol, with k_{obs1} contributing most in wt-VAO, but k_{obs2} contributing most in the Y108F and Y503F variants. Reduction of the Y108F/Y503F variant by chavicol was monitored using single wavelength detection at 439 nm. In this case, the data fit best to a double exponential function. Interestingly, k_{obs1} is in the same range as for the Y108F and Y503F variants, whereas k_{obs2} is an order of magnitude smaller. This brings it into the same range as k_{obs3} observed for wt-VAO and the Y108F and Y503F variants. This provides an explanation for the absence of a third phase, as the decay of the quinone methide intermediate is now likely no longer distinguishable from the second flavin reduction phase. As with Y108F and Y503F, k_{obs2} makes the largest contribution to flavin reduction. For all variants, k_{obs2} lies close to the observed rate of steady-state catalysis, suggesting it is rate-limiting.

Upon reduction of wt-VAO and the Y108F and Y503F variants by 100 μM chavicol at pH 6.2, similar spectral changes were observed as at pH 7.5. Formation of a quinone methide intermediate and concomitant reduction of FAD were followed by the decay of the quinone methide intermediate, which was too slow to be catalytically relevant. The observed reduction rates are given in Table 3. For wt-VAO, the reduction is a biphasic process. The two rates are similar to those observed at pH 7.5, however, as with vanillyl alcohol, the contribution of the rates to the drop in absorbance changes, with k_{obs2} becoming more predominant (a_1:a_2 ≈ 1:2 at pH 6.2 compared with a_1:a_2 ≈ 3:1 at pH 7.5). For the Y108F and Y503F variants, only a single reductive phase was observed, with rate constants that are similar to those of k_{obs2} at pH 7.5, suggesting that the observed rate can be attributed to the same process as k_{obs2} and that the process associated with k_{obs1} does not make an observable contribution to the reduction at pH 6.2. For the Y108F/Y503F variant, the reduction was observed to be biphasic with the rates of the two phases and their relative contributions being similar to those observed at pH 7.5. However, the contribution of the slower phase to the reduction may be underestimated. After reduction of Y108F/Y503F a residual absorbance of 0.03 was measured (usually ~0.015). With the Y108F and Y503F variants it was observed that after the reduction was complete the absorption at 440 nm increased, likely due to the formation of a charge-transfer interaction between the reduced enzyme and a bound substrate molecule. Due to the slow rate of reduction of the Y108F/Y503F variant, formation of such a charge-transfer complex could occur on a similar time scale as the reduction, which would cause part of the absorbance drop associated with the reduction to be masked.

To study the pH dependence of the reaction in more detail, the anaerobic reduction of wt-VAO by 50 μM chavicol was studied in the pH range 6.1–9.5. The overall spectral changes, as monitored using photodiode array detection, were similar to those observed during the experiments presented in Fig. 3 at all pH values. Reduction of FAD and concomitant formation of a quinone methide-reduced enzyme complex was followed by the decay of the quinone methide intermediate to yield the fully reduced enzyme spectrum. As before, the absorption at 440 nm was fit to a triphasic exponential function, yielding two rates that are associated with flavin reduction: k_{obs1} and k_{obs2}. The values of k_{obs1} and k_{obs2} remained similar in this pH range, with the lowest and highest values never differing more than a factor 2 (Fig. 4, *inset*). The pH dependence of the fractional contribution of k_{obs1} to the reduction is shown in Fig. 4. The contribution of k_{obs1} increases with pH. Attempts to fit the data to the Henderson-Hasselbach equation, which allows the determination of the pK_a of an ionizable group were unsuccessful. Although the data display a sigmoidal form, the slope of the sigmoid is lower than described by the Henderson-Hasselbach equation. To estimate the midpoint at which the contribution of k_{obs1} and k_{obs2} to reduction is equal, the data were fit to a sigmoidal curve with the slope as a variable, yielding a midpoint of pH 6.9.

Isoeugenol-binding studies

To evaluate whether the introduced mutations affect the protonation state of phenolic compounds bound to VAO, we studied the binding of the competitive inhibitor isoeugenol to

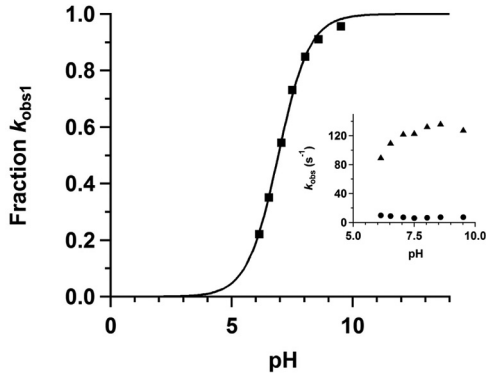

Figure 4. pH dependence of the contribution of k_{obs1} to the reduction of 10 μM wt-VAO by 50 μM chavicol. Anaerobic substrate and enzyme solutions in Britt-Robinson buffers of appropriate pH values were mixed in a stopped-flow apparatus and absorbance changes were monitored using a photodiode array detector. Fitting curves to the absorbance at 440 nm yielded two reduction rates: k_{obs1} (fast) and k_{obs2} (slow). The graph shows the fraction of the drop in absorbance associated with reduction that is contributed by k_{obs1} (fraction $k_{obs1} = a_{obs1}/(a_{obs1}+a_{obs2})$, where a is the amplitude). The *solid line* is a fit of a sigmoidal function to the data, from which a midpoint pH value (fraction k_{obs1} = fraction k_{obs2} = 0.5) of 6.9 was estimated. The *inset* shows the values of k_{obs1} (▲) and k_{obs2} (●). The error on each data point is less than 5%.

the VAO variants. In solution, the phenolic hydroxyl group of isoeugenol has a pK_a of ~10 and its absorption spectrum is dependent on its protonation state (2). In particular, deprotonated isoeugenol displays significantly higher absorption at 320 nm than protonated isoeugenol (ϵ_{320} = 0.21 mM^{-1} cm^{-1} at pH 6 and 8.8 mM^{-1} cm^{-1} at pH 12). Therefore, the absorption of isoeugenol at 320 nm upon binding to VAO can act as a reporter on its protonation state. The pK_a of isoeugenol bound to wt-VAO is ~5 (2). To evaluate whether this has been perturbed by the introduced mutations, the VAO variants were titrated with isoeugenol at pH 7.5. At this pH, isoeugenol is almost entirely protonated in solution, but almost entirely deprotonated when bound to wt-VAO.

Spectral changes observed upon titration of wt-VAO with isoeugenol are shown in Fig. 5. Upon addition of isoeugenol, the intensity of the absorption peak of oxidized FAD at 439 nm decreases, whereas the absorption at wavelengths below 335 nm increases, which is due to the absorption of the added isoeugenol. Plots of the absorption at 439 and 320 nm against the concentration of isoeugenol displayed a curvature indicative of a binding event (Fig. 5, *inset*). The data at each of these wavelengths could be satisfactorily fit to a model assuming a simple 1:1 complex formation between isoeugenol and VAO. This yielded a dissociation constant of 6.8 ± 0.5 μM from the data at 439 nm and 6.8 ± 1.0 μM from the data at 320 nm. The increase in the absorption at 320 nm associated with binding of isoeugenol to VAO is indicative of the fact that, as expected, it is primarily in its deprotonated form upon binding to the enzyme.

Somewhat different spectral changes were observed upon titration of the Y108F variant with isoeugenol (Fig. 5). As with wt-VAO, the intensity of the peak at 439 nm decreases and absorption below 335 nm increases. In addition, a broad absorption band appears at wavelengths between 500 and 680 nm. Such a broad absorption band at high wavelengths is indicative of a charge-transfer interaction between isoeugenol and FAD, likely caused by π-stacking of the aromatic rings of isoeugenol and isoalloxazine. Similar charge-transfer bands have been observed upon binding of various aromatic compounds to the flavoprotein subunit of PCMH (12). Fitting of the data at 439 nm yielded a dissociation constant of 18 ± 2 μM, suggesting binding of isoeugenol is slightly impaired in the Y108F variant as compared with wt-VAO. The absorption at 550 nm also displayed curvature indicative of a single binding event and fitting yielded a dissociation constant of 20 ± 1 μM. This suggests that the drop in absorption at 439 nm and charge-transfer band at wavelengths above 500 nm are both caused by the same binding event, the formation of a 1:1 complex between isoeugenol and Y108F. The absorption at 320 nm, however, did not display the major increase associated with binding to wt-VAO. This suggests that isoeugenol is primarily in its protonated form when bound to Y108F and that the protonated form of isoeugenol forms a charge-transfer complex with the FAD cofactor of Y108F.

For Y503F, the absorption peak at 439 nm also decreased in intensity upon addition of isoeugenol (Fig. 5). Fitting to the data at 439 nm yielded a dissociation constant of 91 ± 7 μM, indicating that binding of isoeugenol is significantly weaker than for wt-VAO. Similar to Y108F, the appearance of a charge-transfer band at wavelengths above 500 nm was observed. However, the measured absorption of this band was too low to reliably determine the dissociation constant. The absorption at 320 nm essentially increased linearly with the isoeugenol concentration, suggesting it is due to the presence of deprotonated isoeugenol in solution and that isoeugenol is predominantly in its protonated form upon binding to Y503F.

With Y108F/Y503F, the results of the titration strongly resemble those with Y108F (Fig. 5). Dissociation constants of 11 ± 1 and 7.0 ± 0.4 μM were obtained by fitting to the data at 439 and 550 nm, respectively. The appearance of a charge-transfer band is observed and the absorption at 320 nm does not show the large increase associated with binding to wt-VAO. This suggests that, like for the Y108F and Y503F variants, isoeugenol is predominantly in its protonated form when in complex with Y108F/Y503F.

Crystal structures

To evaluate the effects of the mutations on the architecture of the active site of VAO, the crystal structures of the Y108F and Y503F variants were solved at 2.8-Å resolution, by molecular replacement using the VAO monomer (PDB code 2VAO) (4) as a search model. Attempts to solve the structure of the Y108F/Y503F variant were hampered by fragility of the crystals. The overall structures of both Y108F and Y503F are essentially identical to that of wt-VAO, as indicated by an r.m.s. deviation of 0.5 Å for 1105 and 1108 pairs of Cα atoms, respectively. The asymmetric unit contains two monomers, which form the functional octamer through crystallographic symmetry, as in wt-VAO.

The geometry of the active site in the mutated enzymes is largely conserved, with the aromatic ring of Phe-108 or Phe-503 located at the same position as the corresponding tyrosine residue in wt-VAO, where they each form a hydrogen bond with the phenolic hydroxyl group of isoeugenol (Fig. 2) (4). Additionally, Tyr-108 interacts with Ser-426 via a hydrogen bond. This interaction is disrupted in the Y108F variant, causing a

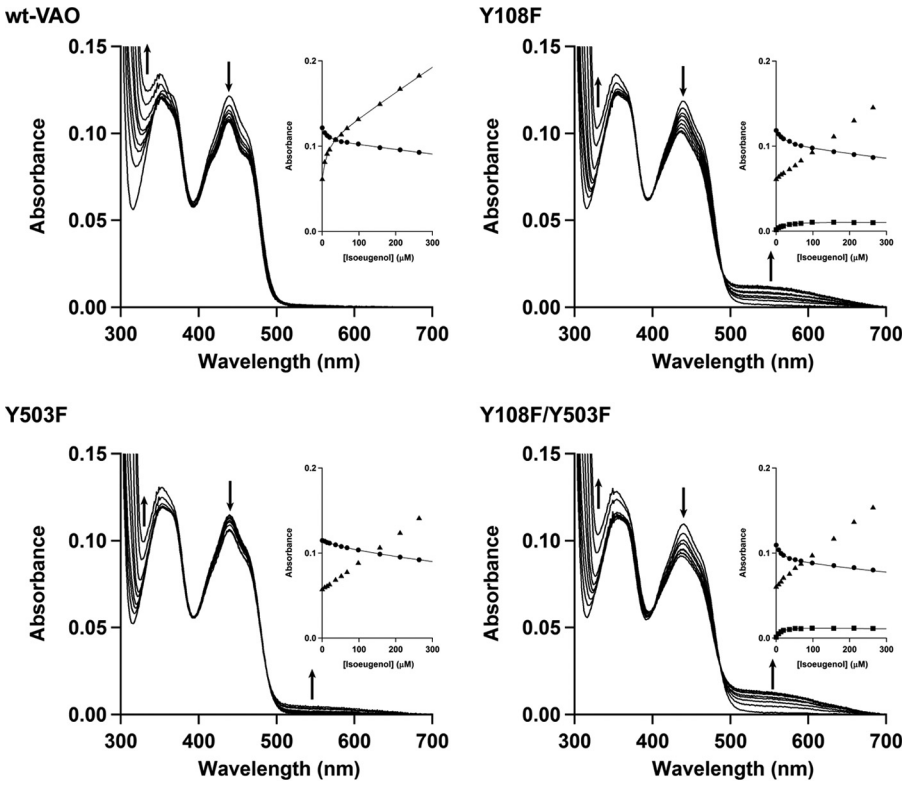

Figure 5. Spectral changes observed upon titration of wt-VAO, Y108F, Y503F, or Y108F/Y503F with the competitive inhibitor isoeugenol. Isoeugenol was added to a 10 μM enzyme solution in 50 mM potassium phosphate buffer, pH 7.5. After each addition, an absorption spectrum was recorded. Spectra recorded at an isoeugenol concentration of 6.6, 13.2, 19.8, 36.0, 51.9, 98.3, 211, and 312 μM are shown. The displayed spectra are corrected for dilution due to the addition of isoeugenol. *Arrows* indicate the direction of the observed changes in absorption upon increasing isoeugenol concentration. *Insets* show the absorption measured at 320 (▲), 439 (●), and 550 (■) nm, with fitted lines used to determine dissociation constants. Absorbance values in these insets are not corrected for dilution.

shift of the Phe-108 side chain toward the FAD cofactor (Fig. 2*B*). In the Y503F variant, the plane of the aromatic ring of Phe-503 is slightly tilted compared with Tyr-503 in wt-VAO (Fig. 2*C*). This may partly be due to the lack of the hydrogen bond between Tyr-503 and Arg-504 that is present in wt-VAO.

In summary, both overall structures of the Y108F and Y503F variants and the geometry of their active sites are extremely similar to wt-VAO. Therefore, changes in reactivity are not due to major structural perturbations, but can be attributed to disruption of the hydrogen bonding capacity conferred by the two tyrosine residues.

Conservation of the phenolate-binding pocket in VAO homologues

To determine whether the residues that form the phenolate-binding pocket in VAO are also present in homologous proteins, we evaluated their conservation in a group of homologues of VAO, EUGO, PCMH, and the related flavocytochrome eugenol hydroxylase from *Pseudomonas* sp. OPS1 (13) that we identified in a previous study and named the 4-phenol oxidizing (4PO) subfamily (14). Additionally, we determined whether they are present in the decarboxylases CndG and FeeG, which catalyze the oxidative decarboxylation of *N*-substituted tyrosine derivatives (15, 16). These enzymes display homology to 4PO subfamily members and catalysis is believed to proceed via a mechanism whereby the initial formation of a *para*-quinone methide intermediate is followed by the expulsion of carbon dioxide. This analysis revealed that Tyr-108, Tyr-503, and Arg-504 are strictly conserved suggesting they are of importance for catalysis in these related enzymes.

Discussion

Our results demonstrate that the presence of at least one of the active site tyrosine residues, Tyr-108 or Tyr-503, is essential for efficient catalysis by VAO, with the k_{cat} values for Y108F/Y503F being less than 2% of those for wt-VAO for each tested substrate. The effect of the single tyrosine to phenylalanine mutations on catalytic efficiency was dependent on the substrate. The oxidation of vanillyl alcohol was severely impaired in both the Y108F and Y503F variants, whereas the oxidation of chavicol was only slightly impaired as compared with wt-VAO.

Stopped-flow kinetics revealed that reduction of the FAD cofactor of VAO by vanillyl alcohol or chavicol proceeds at two distinct rates: k_{obs1} (fast) and k_{obs2} (slow). k_{obs2} lies close to the rate of steady-state catalysis and, therefore, is probably rate-limiting. The observed reduction in the rate of steady-state catalysis for the tyrosine to phenylalanine variants corresponds with the observed reduction in k_{obs2}, demonstrating that impaired flavin reduction is the cause of the reduced rate of catalysis. Titration with the competitive inhibitor isoeugenol indicated that, at pH 7.5, this molecule is predominantly in its deprotonated phenolate anion form when bound to wt-VAO, but predominantly in its protonated form when bound to Y108F, Y503F, or Y108F/Y503F. In combination, these results

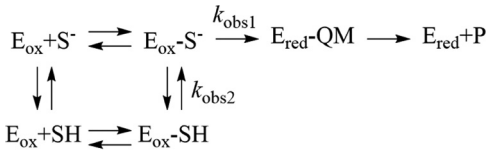

Figure 6. Proposed model for the reductive half-reaction of VAO. Substrates can bind to the enzyme with their phenolic hydroxyl group in its protonated (SH) or deprotonated (S^-) form. Upon binding of the deprotonated form, the enzyme is reduced, yielding the reduced enzyme–quinone methide complex. Reduction by deprotonated substrate corresponds to k_{obs1} from the stopped-flow kinetic experiments presented here. Upon binding of the protonated form, the substrate must be deprotonated to allow flavin reduction to occur, *i.e.* the E_{ox}–SH complex must be converted to the E_{ox}–S^- complex. This corresponds to k_{obs2} from the stopped-flow kinetic experiments. After the reduction, the product is released from the reduced enzyme. This step is too slow to be catalytically relevant, suggesting product release is faster in the presence of dioxygen.

suggest that Tyr-108 and Tyr-503 play a role in activating the substrates of VAO for their reaction with its FAD cofactor by enabling their deprotonation in the active site of the enzyme. Interestingly, the relative contributions of the two reduction rates, k_{obs1} and k_{obs2}, to the change in absorption associated with flavin reduction changes upon the introduction of the tyrosine to phenylalanine mutations. At pH 7.5, k_{obs1} contributes more to the drop in absorption in wt-VAO, whereas in the Y108F, Y503F, and Y108F/Y503F variants, k_{obs2} contributes more to the drop in absorption. The relative contributions of the two rates shift when the reduction is performed at pH 6.2, with the relative contribution of k_{obs2} becoming greater. The reduction of the Y108F/Y503F variant by chavicol was an exception to this observation. However, this may be due to the contribution of k_{obs2} to the reduction at pH 6.2 being underestimated due to the concomitant formation of a charge-transfer interaction between the reduced enzyme and substrate. For the reduction of wt-VAO by chavicol, the contribution of k_{obs1} increases with pH in the pH range 6.1–9.5. The data were fit to a sigmoidal curve with a midpoint pH, at which k_{obs1} and k_{obs2} contribute equally to the reduction, of 6.9.

Based on these results, we propose a somewhat modified model for the reaction mechanism of VAO (Fig. 6). Substrates can bind in the active site of VAO with their phenolic hydroxyl group either in its protonated or deprotonated form. The affinity of the enzyme for the substrate depends on the protonation state of the substrate, with wt-VAO displaying a higher affinity for deprotonated substrates. Subsequently, the substrate reacts with VAO, a reaction that occurs at different rates depending on the protonation state of the substrate. With the deprotonated substrate, the reaction simply involves the transfer of a hydride anion to the FAD cofactor to yield the *para*-quinone methide intermediate. Reaction with the protonated substrate requires the deprotonation of the phenolic hydroxyl group of the substrate either prior to or at the same time as the hydride-transfer reaction. The proton is transferred to either Tyr-108 or Tyr-503, which may be transiently deprotonated in the active site of the enzyme. This is stimulated by Arg-504, which is positioned so as to form a cation-π interaction with Tyr-108, lowering its pK_a. This model explains the two rates of flavin reduction observed for each substrate, with k_{obs1} representing the reaction with deprotonated substrate and k_{obs2} representing the reaction with protonated substrate. This is supported by the fact that the contribution of k_{obs1} to flavin reduction increases with pH, as at higher pH values a larger percentage of the substrate is in its deprotonated form. The results of the isoeugenol titrations support the idea that substrates bind to Y108F, Y503F, and Y108F/Y503F predominantly in their protonated form at pH 7.5, as opposed to wt-VAO where it predominantly binds in its deprotonated form. This explains the change in the relative contributions of k_{obs1} and k_{obs2} to flavin reduction upon introduction of the tyrosine to phenylalanine mutations. The mutations prevent the preferential binding of the deprotonated form of the substrates observed with wt-VAO due to the loss of hydrogen-bonding interactions that stabilize the negative charge on the phenolate oxygen. In support of this, the crystallographic analysis revealed that, although the mutations do not produce any major structural perturbation of the active site architecture, they modify the hydrogen-bonding network that is essential to activate the substrate for the reaction with the flavin cofactor. The fact that the curve of the fractional contribution of k_{obs1} to the reduction *versus* pH does not obey the Henderson-Hasselbach equation may be attributable to the effects of functional groups near the phenolic hydroxyl group on its protonation state, which can have a distorting effect on the titration behavior of ionizable groups in proteins (17). Additionally, interconversion of the enzyme-protonated substrate (E_{ox}–SH) and enzyme-deprotonated substrate (E_{ox}–S^-) complexes may involve more significant changes than simply the deprotonation of the phenolic hydroxyl group of the substrate. The fact that a charge-transfer interaction is observed between the enzyme and protonated isoeugenol during titrations with this molecule, but not between the enzyme and deprotonated isoeugenol, suggest that the ligand may bind to the enzyme in a slightly different conformation depending on its protonation state. Thus conversion of the E_{ox}–SH complex to the E_{ox}–S^- complex may require a reorientation of the substrate within the active site, and possibly minor changes in the conformation of active site residues. This could explain the reasonably low rates observed for k_{obs2}. Although in our view this model provides the most satisfactory explanation of our observations, an alternative mechanism where the two observed reduction rates reflect the presence of two forms of the enzyme, one in which both Tyr-108 and Tyr-503 are protonated and one in which one of the two tyrosine residues is deprotonated, cannot be fully ruled out.

The effect of the single Y108F and Y503F mutations on the rate of reduction of VAO was dependent on the substrate used. With the benzylic alcohol vanillyl alcohol, a far more severe drop in both k_{obs1} and k_{obs2} was observed than with the 4-allylphenol chavicol. However, the change in the relative contributions of k_{obs1} and k_{obs2} to flavin reduction is similar. Possibly, the large effect on the reduction rate seen with vanillyl alcohol is due to incorrect positioning of the substrate in the active site of Y108F and Y503F. Hydrogen bonds between the phenolic hydroxyl group of the substrate and the two tyrosine residues may be of importance in maintaining it in the correct orientation for the hydride-transfer reaction to take place. This effect may be less important for chavicol than for vanillyl alcohol, as interactions involving its longer side chain may lock it into position in the active site. In this context, it is interesting to note

that the K_m for the oxidation of chavicol by wt-VAO is significantly lower than that for the oxidation of vanillyl alcohol, indicating tighter binding of chavicol.

In addition to the 4PO subfamily members mentioned above, a catalytic motif composed of two tyrosine residues has been proposed to be involved in substrate activation in other enzymes in which catalysis proceeds through a *para*-quinone methide intermediate, such as the cofactor-independent hydroxycinnamoyl-CoA hydratase-lyase from *Pseudomonas fluorescens* AN103 (18) and bacterial phenolic acid decarboxylases (19) (although an alternative mechanism has also been proposed (20, 21)). This suggests that these structurally unrelated proteins have obtained similar mechanisms for the activation of the phenolic hydroxyl groups of their substrates through convergent evolution.

Catalytic motifs composed of two tyrosine residues have also been implicated in substrate activation in a number of enzymes that catalyze oxidation reactions that do not involve a *para*-substituted phenol. They have been proposed to facilitate the activation of hydroxyl groups for their oxidation to carbonyls in other oxidoreductases from the VAO/PCMH family, such as aclacinomycin oxidoreductase from *Streptomyces galilaeus* ATCC 31615 (22), Dbv29 from *Nonomuraea* sp. ATCC 39727 (23), GilR from *Streptomyces griseoflavus* (24), and the monolignol oxidoreductase BBE-like protein 15 from *Arabidopsis thaliana* (25). These enzymes all belong to the same clade of the VAO/PCMH family, which primarily contains enzymes with a bicovalently bound FAD cofactor (26). Despite their homology with VAO, a sequence and structural alignment of the five proteins demonstrated that the tyrosine pair found in these enzymes is not equivalent to that found in VAO, suggesting the motifs evolved separately.

In summary, the results presented here indicate that two tyrosine residues, Tyr-108 and Tyr-503, are responsible for activating the phenolic substrates of VAO for oxidation by facilitating the binding of their deprotonated phenolate form in the active site, shedding light on the catalytic mechanism of VAO and other homologous flavoenzymes that oxidize *para*-substituted phenols.

Experimental procedures

Materials

Vanillyl alcohol and isoeugenol were from Sigma. Chavicol was from Quest International (Naarden, NL). All other chemicals were from commercial sources and of the purest grade available.

Cloning, protein expression, and purification

Constructs encoding for the Y108F and Y503F variants were created by linear whole-plasmid amplification from the pBC11 (27) plasmid using the mutagenic primers CATCTCTATTGGAAGGAATTCCGGAT*TT*GGCGGTGCTGCGCC (Y108F) and ATGGATGGGGCGAAT*TT*CGAACCCATCTGGC (Y503F) (nucleotides in italics are the sites of mutation for introduction of the tyrosine to phenylalanine mutations, the underlined nucleotide indicates the site of a silent mutation that introduces an EcoRI site). After amplification and concomitant ligation, template DNA was digested using DpnI and the mutagenized plasmids were transformed into DH5α *E. coli*. Correct plasmids, as confirmed by sequencing, were transformed into BL21 *E. coli* for protein expression. The construct encoding for the Y108F/Y503F variant was created in a similar manner, using the plasmid encoding for the Y108F variant as the template for amplification and the primer for the Y503F variant. All variants were expressed and purified as described previously for wt-VAO (14).

Analytical methods

Unless specified otherwise, all experiments were performed in 50 mM potassium phosphate buffer, pH 7.5. Absorption spectra of purified proteins were recorded using a Hewlett Packard 8453 photodiode array spectrophotometer (Agilent Technologies, Santa Clara, CA) and enzyme concentrations were determined using the extinction coefficient of wt-VAO at 439 nm (ϵ_{439} = 12,500 M^{-1} cm^{-1} (1)). For trichloroacetic acid precipitations, 5% (w/v) trichloroacetic acid was mixed with 10 μM enzyme and samples were incubated on ice for 30 min. Subsequently, the precipitated protein was pelleted by centrifugation (21,000 × *g*, 15 min, 4 °C), and the presence of FAD in the pellet or supernatant was judged from its color. The absence of FAD from the supernatants was confirmed by measuring their absorption spectra. Analytical gel filtration was performed using a Superdex 200 HR 10/30 column on an Äkta pure chromatography system (GE Healthcare). Samples of enzyme at a concentration of 10 μM were loaded onto the column and subsequently eluted in 50 mM potassium phosphate buffer, pH 7.5, containing 150 mM potassium chloride. Molecular masses were determined based on a calibration curve of proteins of known mass. Thermal unfolding of the VAO variants was monitored by the ThermoFAD method (11) using a MiniOpticon real-time PCR system (Bio-Rad). Protein solutions at a concentration of 7 μM were subjected to a temperature gradient from 25 to 70 °C and the fluorescence of the FAD cofactor was measured every 0.5 °C with excitation and emission wavelengths of 485 ± 30 and 625 ± 30 nm, respectively. Thermal midpoints of unfolding were determined by finding the maximum of the derivative of the unfolding curves.

Steady-state kinetics

All experiments were performed at 25 °C in 50 mM potassium phosphate buffer, pH 7.5. The oxidation of vanillyl alcohol to vanillin was followed by monitoring the absorption of the product at 340 nm (ϵ_{340} = 14,000 M^{-1} cm^{-1}). The oxidation of chavicol was followed by monitoring oxygen consumption using a Hansatech Oxytherm system (Hansatech Instruments, King's Lynn, UK). Steady-state kinetic parameters were determined by fitting the obtained data to the Michaelis-Menten equation (vanillyl alcohol) using IGOR Pro (Wavemetrics, Lake Oswego, OR) or to a modified version of the Michaelis-Menten equation that includes a term to take substrate inhibition into account (chavicol),

$$k_{obs} = \frac{k_{cat} \times [S]}{K_m + [S] + \frac{[S]^2}{K_i}} \quad \text{(Eq. 1)}$$

where k_{obs} is the measured initial rate, k_{cat} is the turnover number, K_m is the Michaelis constant, K_i is the inhibition constant for substrate inhibition, and [S] is the substrate concentration.

Stopped-flow kinetics

The reduction of VAO variants by vanillyl alcohol or chavicol was followed using an SX20 stopped-flow system (Applied Photophysics, Leatherhead, UK) equipped with a photodiode array detector or a photomultiplier detector as applicable. Enzyme and substrate solutions in 50 mM potassium phosphate buffer, pH 6.2 or 7.5, as appropriate, containing 5 mM glucose were made anaerobic by first flushing them with nitrogen gas for 10 min and then adding 0.3 μM glucose oxidase. Subsequently, the enzyme and substrate solutions were mixed to final concentrations of 10 μM enzyme and 2 mM (vanillyl alcohol) or 100 μM (chavicol) substrate and spectral changes were monitored at 25 °C. Rate constants were obtained by global fitting of multiple single wavelength traces to appropriate exponential functions using IGOR Pro. Spectral deconvolution of multiwavelength data were performed using Pro-Kineticist (Applied Photophysics). To study the pH dependence of the reduction of wt-VAO by chavicol in more detail, the reaction was performed at various pH values in the pH range 6.1–9.5. Experiments were performed in Britt-Robinson buffers consisting of 40 mM acetic acid, 40 mM phosphoric acid, and 40 mM boric acid set to the correct pH using potassium hydroxide. The ionic strength of the buffers was set to 0.2 M by the addition of potassium sulfate. Subsequently, enzyme and substrate solutions were made anaerobic as described above, mixed to final concentrations of 10 μM enzyme and 50 μM chavicol, and the reduction was monitored at 25 °C and data were analyzed as described above.

Isoeugenol-binding studies

Changes in the spectral properties of the VAO variants upon binding of the competitive inhibitor isoeugenol were monitored using a Cary 4000 spectrophotometer (Agilent Technologies, Santa Clara, CA). Isoeugenol was titrated to 10 μM enzyme in 50 mM potassium phosphate buffer, pH 7.5, and an absorption spectrum was recorded after every addition. Dissociation constants were determined by fitting the data at a specific wavelength to a model assuming formation of a 1:1 enzyme–isoeugenol complex using the following formula with IGOR Pro,

$$A = \epsilon_E \times [E]_f + \epsilon_{EI} \times [EI] + \epsilon_I \times [I]_f \quad \text{(Eq. 2)}$$

where

$$[EI] = \frac{[E]_t + [I]_t + K_d - \sqrt{([E]_t + [I]_t + K_d)^2 - 4 \times [I]_t \times [E]_t}}{2} \quad \text{(Eq. 3)}$$

and

$$[E]_f = [E]_t - [EI] \quad \text{(Eq. 4)}$$

Table 4
Data collection and refinement statistics

	Y108F	Y503F
PDB code	5MXJ	5MXU
Space group	*I*4	*I*4
Resolution (Å)	2.8	2.8
a, *b*, *c* (Å)	137.9, 137.9, 132.9	138.0, 138.0, 132.9
R_{sym} [a,b,c] (%)	8.7 (67.9)	10.1 (63.8)
$CC_{1/2}$ [a,c]	0.99 (0.54)	0.99 (0.54)
Completeness[b] (%)	89.7 (91.9)	91.8 (94.3)
Unique reflections	27138	27846
Multiplicity[c]	2.3 (2.1)	2.4 (2.4)
I/σ[c]	9.0 (1.3)	7.0 (1.3)
Number of atoms		
Protein	8697	8706
FAD/glycerol/water	2 × 53/3 × 6/260	2 × 53/2 × 6/232
Average *B* value for all atoms (Å^2)	52.1	52.6
R_{cryst} [c,d] (%)	18.0 (34.2)	17.5 (30.2)
R_{free} [c,d] (%)	25.9 (33.7)	24.9 (37.4)
R.m.s. bond length (Å)	0.01	0.01
R.m.s. bond angles (°)	1.56	1.48
Ramachandran outliers (%)	0	0

[a] Data processing statistics was based on $CC_{1/2}$ as described in Refs. 34 and 35.
[b] $R_{sym} = \Sigma|I_i - \langle I\rangle|/\Sigma I_i$, where I_i is the intensity of *i*th observation and $\langle I\rangle$ is the mean intensity of the reflection.
[c] Values in parentheses are for reflections in the highest resolution shell.
[d] $R_{cryst} = \Sigma||F_{obs}| - |F_{calc}||/\Sigma|F_{obs}|$, where F_{obs} and F_{calc} are the observed and calculated structure factor amplitudes, respectively. R_{cryst} and R_{free} were calculated using the working and test sets, respectively.

and

$$[I]_f = [I]_t - [EI] \quad \text{(Eq. 5)}$$

with ϵ_E, ϵ_{EI}, and ϵ_I being the molar extinction coefficients of the free enzyme, the enzyme-inhibitor complex, and the free inhibitor, respectively, $[E]_f$ being the concentration of free enzyme, $[EI]$ the concentration of enzyme-inhibitor complex, $[I]_f$ the concentration of free inhibitor, $[E]_t$ the total enzyme concentration, $[I]_t$ the total inhibitor concentration, and K_d the dissociation constant.

Crystallization and structure determination

VAO variants were crystallized by the hanging drop vapor diffusion method. Protein solutions at a concentration of 180–220 μM in 50 mM potassium phosphate buffer, pH 7.5, were mixed 1:1 (v/v) with a mother liquor containing 6% (w/v) PEG4000 in 100 mM sodium acetate buffer, pH 4.6, and equilibrated against the mother liquor at 20 °C. Prior to data collection, crystals were transferred to a cryoprotectant solution containing 10% (w/v) PEG4000 and 20% (w/v) glycerol in 100 mM sodium acetate buffer, pH 4.6, and cryo-cooled in liquid nitrogen. X-ray diffraction data were collected at the X06DA beamline of the Swiss Light Synchrotron in Villigen, Switzerland (SLS), and at the ID30B beamline of the European Synchrotron Radiation Facility in Grenoble, France (ESRF). Images were integrated using MOSFLM (28) and data were scaled using programs of the CCP4 suite (29). Detailed data processing statistics are shown in Table 4. Structures of VAO mutants were solved by molecular replacement using PHASER (30) with the structure of wt-VAO (PDB code 2VAO (4)) devoid of all ligands and water molecules as a search model. Subsequently, structures were refined by alternating refinement using REFMAC5 (31) and manual model building using COOT (32). Figures were prepared with CCP4mg (33). Atomic coordinates and structure factors were deposited in

the Protein Data Bank under the PDB ID codes 5MXJ (Y108F-VAO) and 5MXU (Y503F-VAO).

Author contributions—T. A. E. and W. J. H. B. conceived the study and designed the experiments. T. A. E. and R. C. A. performed the expression, purification, and biochemical characterization of the VAO variants. T. A. E. and Q. T. N. performed the crystallization and solved the structures of the VAO variants. A. M. and C. B. supervised this part of the study. T. A. E. performed the stopped-flow kinetics measurements. E. R. and M. W. F. supervised this part of the study. G. G. performed the bioinformatic analysis. All authors contributed to analyzing the data and writing the paper.

Acknowledgments—We thank the European Synchrotron Radiation Facility (ESRF) and the Swiss Light Source (SLS) for providing beam time and assistance and the European Community's Seventh Framework Programme (FP7/2007–2013) under BioStruct-X (Grants 7551 and 10205) for funding synchrotron trips.

References

1. de Jong, E., van Berkel, W. J., van der Zwan, R. P., and de Bont, J. A. (1992) Purification and characterization of vanillyl-alcohol oxidase from *Penicillium simplicissimum*: a novel aromatic alcohol oxidase containing covalently bound FAD. *Eur. J. Biochem.* **208,** 651–657
2. Fraaije, M. W., Veeger, C., and van Berkel, W. J. (1995) Substrate specificity of flavin-dependent vanillyl-alcohol oxidase from *Penicillium simplicissimum*: evidence for the production of 4-hydroxycinnamyl alcohols from 4-allylphenols. *Eur. J. Biochem.* **234,** 271–277
3. van den Heuvel, R. H., Fraaije, M. W., Laane, C., and van Berkel, W. J. (1998) Regio- and stereospecific conversion of 4-alkylphenols by the covalent flavoprotein vanillyl-alcohol oxidase. *J. Bacteriol.* **180,** 5646–5651
4. Mattevi, A., Fraaije, M. W., Mozzarelli, A., Olivi, L., Coda, A., and van Berkel, W. J. (1997) Crystal structures and inhibitor binding in the octameric flavoenzyme vanillyl-alcohol oxidase: the shape of the active-site cavity controls substrate specificity. *Structure* **5,** 907–920
5. Fraaije, M. W., Van Berkel, W. J., Benen, J. A., Visser, J., and Mattevi, A. (1998) A novel oxidoreductase family sharing a conserved FAD-binding domain. *Trends Biochem. Sci.* **23,** 206–207
6. Fraaije, M. W., and van Berkel, W. J. (1997) Catalytic mechanism of the oxidative demethylation of 4-(methoxymethyl)phenol by vanillyl-alcohol oxidase: evidence for formation of a *p*-quinone methide intermediate. *J. Biol. Chem.* **272,** 18111–18116
7. Fraaije, M. W., van den Heuvel, R. H., Roelofs, J. C., and van Berkel, W. J. (1998) Kinetic mechanism of vanillyl-alcohol oxidase with short-chain 4-alkylphenols. *Eur. J. Biochem.* **253,** 712–719
8. Nguyen, Q.-T., de Gonzalo, G., Binda, C., Rioz-Martínez, A., Mattevi, A., and Fraaije, M. W. (2016) Biocatalytic properties and structural analysis of eugenol oxidase from *Rhodococcus jostii* RHA1: a versatile oxidative biocatalyst. *ChemBioChem* **17,** 1359–1366
9. Cunane, L. M., Chen, Z.-W., Shamala, N., Mathews, F. S., Cronin, C. N., and McIntire, W. S. (2000) Structures of the flavocytochrome *p*-cresol methylhydroxylase and its enzyme-substrate complex: gated substrate entry and proton relays support the proposed catalytic mechanism. *J. Mol. Biol.* **295,** 357–374
10. Efimov, I., Cronin, C. N., Bergmann, D. J., Kuusk, V., and McIntire, W. S. (2004) Insight into covalent flavinylation and catalysis from redox, spectral, and kinetic analyses of the R474K mutant of the flavoprotein subunit of *p*-cresol methylhydroxylase. *Biochemistry* **43,** 6138–6148
11. Forneris, F., Orru, R., Bonivento, D., Chiarelli, L. R., and Mattevi, A. (2009) ThermoFAD, a Thermofluor®-adapted flavin ad hoc detection system for protein folding and ligand binding. *FEBS J.* **276,** 2833–2840
12. Engst, S., Kuusk, V., Efimov, I., Cronin, C. N., and McIntire, W. S. (1999) Properties of *p*-cresol methylhydroxylase flavoprotein overproduced by *Escherichia coli*. *Biochemistry* **38,** 16620–16628
13. Brandt, K., Thewes, S., Overhage, J., Priefert, H., and Steinbüchel, A. (2001) Characterization of the eugenol hydroxylase genes (*ehyA*/*ehyB*) from the new eugenol-degrading *Pseudomonas* sp. strain OPS1. *Appl. Microbiol. Biotechnol.* **56,** 724–730
14. Ewing, T. A., Gygli, G., and van Berkel, W. J. (2016) A single loop is essential for the octamerization of vanillyl alcohol oxidase. *FEBS J.* **283,** 2546–2559
15. Brady, S. F., Chao, C. J., and Clardy, J. (2002) New natural product families from an environmental DNA (eDNA) gene cluster. *J. Am. Chem. Soc.* **124,** 9968–9969
16. Rachid, S., Revermann, O., Dauth, C., Kazmaier, U., and Müller, R. (2010) Characterization of a novel type of oxidative decarboxylase involved in the biosynthesis of the styryl moiety of chondrochloren from an acylated tyrosine. *J. Biol. Chem.* **285,** 12482–12489
17. Ullmann, G. M., and Bombarda, E. (2013) pK_a values and redox potentials of proteins: what do they mean? *Biol. Chem.* **394,** 611–619
18. Bennett, J. P., Bertin, L., Moulton, B., Fairlamb, I. J., Brzozowski, A. M., Walton, N. J., and Grogan, G. (2008) A ternary complex of hydroxycinnamoyl-CoA hydratase-lyase (HCHL) with acetyl-CoA and vanillin gives insights into substrate specificity and mechanism. *Biochem. J.* **414,** 281–289
19. Sheng, X., Lind, M. E., and Himo, F. (2015) Theoretical study of the reaction mechanism of phenolic acid decarboxylase. *FEBS J.* **282,** 4703–4713
20. Rodríguez, H., Angulo, I., de Las Rivas, B., Campillo, N., Páez, J. A., Muñoz, R., and Mancheño, J. M. (2010) *p*-Coumaric acid decarboxylase from *Lactobacillus plantarum*: structural insights into the active site and decarboxylaction catalytic mechanism. *Proteins* **78,** 1662–1676
21. Frank, A., Eborall, W., Hyde, R., Hart, S., Turkenburg, J. P., and Grogan, G. (2012) Mutational analysis of phenolic acid decarboxylase from *Bacillus subtilis* (BsPAD), which converts bio-derived phenolic acids to styrene derivatives. *Catal. Sci. Technol.* **2,** 1568–1574
22. Alexeev, I., Sultana, A., Mäntsälä, P., Niemi, J., and Schneider, G. (2007) Aclacinomycin oxidoreductase (AknOx) from the biosynthetic pathway of the antibiotic aclacinomycin is an unusual flavoenzyme with a dual active site. *Proc. Natl. Acad. Sci. U.S.A.* **104,** 6170–6175
23. Liu, Y.-C., Li, Y.-S., Lyu, S.-Y., Hsu, L.-J., Chen, Y.-H., Huang, Y.-T., Chan, H.-C., Huang, C.-J., Chen, G.-H., Chou, C.-C., Tsai, M.-D., and Li, T.-L. (2011) Interception of teicoplanin oxidation intermediates yields new antimicrobial scaffolds. *Nat. Chem. Biol.* **7,** 304–309
24. Noinaj, N., Bosserman, M. A., Schickli, M. A., Piszczek, G., Kharel, M. K., Pahari, P., Buchanan, S. K., and Rohr, J. (2011) The crystal structure and mechanism of an unusual oxidoreductase, GilR, involved in gilvocarcin V biosynthesis. *J. Biol. Chem.* **286,** 23533–23543
25. Daniel, B., Pavkov-Keller, T., Steiner, B., Dordic, A., Gutmann, A., Nidetzky, B., Sensen, C. W., van der Graaff, E., Wallner, S., Gruber, K., and Macheroux, P. (2015) Oxidation of monolignols by members of the berberine bridge enzyme family suggests a role in plant cell wall metabolism. *J. Biol. Chem.* **290,** 18770–18781
26. Leferink, N. G., Heuts, D. P., Fraaije, M. W., and van Berkel, W. J. (2008) The growing VAO flavoprotein family. *Arch. Biochem. Biophys.* **474,** 292–301
27. van den Heuvel, R. H., Fraaije, M. W., Mattevi, A., and van Berkel, W. J. (2000) Asp-170 is crucial for the redox properties of vanillyl-alcohol oxidase. *J. Biol. Chem.* **275,** 14799–14808
28. Battye, T. G., Kontogiannis, L., Johnson, O., Powell, H. R., and Leslie, A. G. (2011) iMOSFLM: a new graphical interface for diffraction-image processing with MOSFLM. *Acta Crystallogr. D Biol. Crystallogr.* **67,** 271–281
29. Winn, M. D., Ballard, C. C., Cowtan, K. D., Dodson, E. J., Emsley, P., Evans, P. R., Keegan, R. M., Krissinel, E. B., Leslie, A. G., McCoy, A., McNicholas, S. J., Murshudov, G. N., Pannu, N. S., Potterton, E. A., Powell, H. R., *et al.* (2011) Overview of the CCP4 suite and current developments. *Acta Crystallogr. D Biol. Crystallogr.* **67,** 235–242

30. McCoy, A. J., Grosse-Kunstleve, R. W., Adams, P. D., Winn, M. D., Storoni, L. C., and Read, R. J. (2007) Phaser crystallographic software. *J. Appl. Crystallogr.* **40,** 658–674
31. Murshudov, G. N., Vagin, A. A., and Dodson, E. J. (1997) Refinement of macromolecular structures by the maximum-likelihood method. *Acta Crystallogr. D Biol. Crystallogr.* **53,** 240–255
32. Emsley, P., and Cowtan, K. (2004) Coot: Model-building tools for molecular graphics. *Acta Crystallogr. D Biol. Crystallogr.* **60,** 2126–2132
33. McNicholas, S., Potterton, E., Wilson, K. S., and Noble, M. E. (2011) Presenting your structures: the CCP4mg molecular-graphics software. *Acta Crystallogr. D Biol. Crystallogr.* **67,** 386–394
34. Karplus, P. A., and Diederichs, K. (2012) Linking crystallographic model and data quality. *Science* **336,** 1030–1033
35. Karplus, P. A., and Diederichs, K. (2015) Assessing and maximizing data quality in macromolecular crystallography. *Curr. Opin. Struct. Biol.* **34,** 60–68

Two tyrosine residues, Tyr-108 and Tyr-503, are responsible for the deprotonation of phenolic substrates in vanillyl-alcohol oxidase

Tom A. Ewing, Quoc-Thai Nguyen, Robert C. Allan, Gudrun Gygli, Elvira Romero, Claudia Binda, Marco W. Fraaije, Andrea Mattevi and Willem J. H. van Berkel

J. Biol. Chem. 2017, 292:14668-14679.
doi: 10.1074/jbc.M117.778449 originally published online July 17, 2017